

Regular article

A molecular dynamics study on Rh^{3+} hydration: development and application of a first principles hydrated ion–water interaction potential

José M. Martínez¹, Patrick J. Merkling¹, Rafael R. Pappalardo¹, Keith Refson², Enrique Sánchez Marcos¹

¹ Departamento de Química Física, Universidad de Sevilla, 41012- Seville, Spain

² Rutherford Appleton Laboratory, Chilton Didcot Oxfordshire OX11 0QX, UK

Received: 25 February 2003 / Accepted: 30 April 2003 / Published online: 27 November 2003

© Springer-Verlag 2003

Abstract. The Rh^{3+} aquaion exhibits one of the largest residence times of water molecules in the first hydration shell. The extreme stability of this hexahydrated ion in water solutions makes Rh^{3+} an extremely suitable candidate to be studied using the hydrated ion model. According to this approach, the representative cationic entity in aqueous solution is the ion plus its first hydration shell (i.e. the hydrated ion) and not the bare ion. Our group has successfully applied that concept in the framework of classical statistical simulations based on first principles ion–water interaction potentials. The methodology is now applied to the $[\text{Rh}(\text{H}_2\text{O})_6]^{3+}$ case based on a previous generalization in which some of the contributions were found to be transferable among the cases already studied (Cr^{3+} , Al^{3+} , Mg^{2+} , Be^{2+}). In this contribution a flexible hydrate model is presented, in which rigid first-shell water molecules have rotational and translational degrees of freedom, allowing for internal dynamics of the hydrated ion entity. The potential presented is thoroughly tested by means of a set of molecular dynamics simulations. Structural, dynamical, energetic and spectroscopic information is retrieved from the simulations, allowing the estimation of properties such as ion hydration energy, vibrational spectra of the intermolecular modes, cation mobility, rotational dynamics of the hydrated ion and first-shell water molecules and residence times of the second-shell water molecules. Extension of the Ewald sum to terms r^{-4} , r^{-6} and r^{-7} is presented and applied to systems of different size $([\text{Rh}(\text{H}_2\text{O})_6]^{3+} + (n - 6)\text{H}_2\text{O}, n = 50, 100, 200, 500, 1000 \text{ and } 2500)$ and cutoff radii.

Keywords: Rh(III) aquaion – Radial distribution function – Cation mobility – Extended Ewald sum

Contribution to the Jacopo Tomasi Honorary Issue

Correspondence to: E.S. Marcos
e-mail: sanchez@simulux.us.es

1 Introduction

Metal ions in solution is a classical topic of physical chemistry that is experiencing a renewed interest owing to the large number of chemical, environmental and biochemical properties directly related to their physico-chemical behavior [1, 2, 3, 4].

The rationalization of the properties of metal ions in solution benefits from theoretical studies which provide independent pieces of information either within a microscopic or within a macroscopic framework [4]. Among them, computer simulations have gained increasing popularity as far as they provide a relatively simple procedure to model disordered systems containing a large number of particles interacting by means of no simple forces [5, 6]. In addition, the current computational resources allow the simulation of systems with a large number of particles (of the order of thousands) and long simulation times (of the order of tens of nanoseconds). One of the key points of these types of computations is the definition of the intermolecular potentials employed [7]. If they are based on ab initio calculations, the simulations are nonempirical and strategies of systematic improvements of the potentials are easier to design [5]. These advantages are partially counterbalanced by the fact that when charged particles, such as metal ions, interact in the presence of polarizable molecules with complex structures, such as water, phenomena associated with the collective interaction of particles are relevant, and then many-body effects have to be included in the development of potentials [8, 9]. As a consequence, the simple quantum mechanical description of an ion–water potential-energy surface is not enough to obtain an accurate intermolecular potential.

A practical strategy to deal with this problem is to recover the concept of the hydrated ion from ionic electrochemistry. In that field, it has long been recog-

nized that ions and especially highly charged monoatomic cations, M^{m+} , behave in solutions of water or other polar solvents, S , as molecular complexes $[M(S)_n]^{m+}$ called solvated ions [10, 11]. In the case of water, the hydrated ion is a peculiar entity in which water molecules behave rather as ligands of a coordination complex, showing partial charge transfer and strong polarization [12, 13]. Our group implemented this idea within statistical simulations by developing ab initio $[M(\text{H}_2\text{O})_6]^{m+}-\text{H}_2\text{O}$ intermolecular potentials [14]. Thus, the ion interacts in aqueous solution via its hydrated form. The current application of this strategy is limited by the fact that no water exchange in the first hydration shell is allowed, since two different types of water molecules are defined, although ongoing developments could overcome such limitations. As a consequence, the method should be applied only to hydrated ions of high stability, that is, those with mean residence times of first-shell water molecules long enough compared to the simulation time. This requirement is fulfilled by metal cations, such as Cr^{3+} , Al^{3+} , Mg^{2+} and Be^{2+} [15], whose potentials were built previously [16, 17, 18] and tested, supporting the proposed methodology [19, 20, 21, 22].

This work is devoted to Rh^{3+} hydration. The Rh^{3+} aquaion shows, together with Ir^{3+} , the largest residence time of water molecules in the first hydration shell (approximately 10 years) [13, 23, 24]. The extreme stability of this hexahydrated ion in water solutions makes Rh^{3+} an extremely suitable candidate to be studied under the framework of the hydrated ion model. A new set of ab initio interaction potentials for Rh^{3+} is presented, and is tested by carrying out classical molecular dynamics (MD) simulations. Energetic, structural and dynamical properties are extracted from the analysis of these simulations. Special attention is paid in this work to two methodological points. The first one concerns the inclusion within the Ewald sum method of the terms corresponding to r^{-4} , r^{-6} and r^{-7} , in addition to the usual r^{-1} . It must reduce the energy correction term owing to the truncation of the potential at the cutoff radius employed, providing at the same time more accurate forces. The second point derived from the previous one is the evaluation of the behavior of the ion hydration energy as a function of the system size, here including the use of different cutoff radii.

2 Methodology

In this section, details about the quantum mechanical computations for the Rh^{3+} -water potential energy surface are given, the hydrated ion model of interaction potentials is briefly outlined, emphasizing the particular application of the Rh^{3+} , and the methodology developed to apply the Ewald-like treatment of r^{-n} practically in a MD code is summarized.

2.1 Quantum-mechanical calculations

The reference structure for $[\text{Rh}(\text{H}_2\text{O})_6]^{3+}$ is obtained by an optimization at the MP2 level, using the Stuttgart/Dresden relativistic effective core potential for the Rh atom [25]. The sdd basis sets were used for the Rh atom, and correlation-consistent polarized valence basis sets of double- ζ augmented by diffuse

functions (aug-cc-pVDZ) were used for the other atoms [26, 27]. At this level, the optimized geometrical parameters of the hydrate are: $R(\text{Rh}-\text{O}) = 2.003 \text{ \AA}$, $R(\text{O}-\text{H}) = 0.977 \text{ \AA}$ and $\angle\text{HOH} = 109.6^\circ$. The structure has T_h symmetry.

Bulk effects on the hydrated ion were included by means of the continuum solvation model [28], which accounts for the average polarization induced on the hydrate charge distribution by the condensed medium. The polarizable continuum model (PCM) method developed by Tomasi's group [28, 29] was used in its integral equation formalism (IEFPCM) [30, 31] as implemented in the Gaussian 98 program [32, 33]. For O and H atoms, the standard radii [34] were used, $R_{\text{O}} = 1.68 \text{ \AA}$ and $R_{\text{H}} = 1.44 \text{ \AA}$. For the Rh atom several radii were tested in order to guarantee good behavior of solvent effects computations, $R_{\text{Rh}} = 2.0 \text{ \AA}$. Thus, the hydrated ion-water (HIW) and ion-water first-shell (IW1) potentials use effective atomic electrostatic charges derived from a fitting procedure that reproduces the molecular electrostatic potential generated by the hydrate's wavefunction already polarized by the dielectric continuum. In practice, the Sigfridsson-Ryde recommendation [35] was applied to the Merz-Kollman method [36] in order to obtain the charges on the different sites of the hydrate (values of q_{Rh} , q_{O} and q_{H} are given in the next section).

2.2 Outline of the hydrated ion model

Interactions of the metal cation in aqueous solutions are described by means of two intermolecular potentials. The first one is called the HIW [14, 17] potential and accounts for the interaction between the hydrated ion and a bulk water molecule, $[M(\text{H}_2\text{O})_n]^{m+}-\text{H}_2\text{O}$. The potential adopts a site-site form involving the following analytical expression:

$$E_{\text{HIW}} = \sum_i^{\text{HI sites}} \sum_j^{\text{W sites}} \frac{A_4^{ij}}{r_{ij}^4} + \frac{A_6^{ij}}{r_{ij}^6} + \frac{A_{12}^{ij}}{r_{ij}^{12}} + \frac{q_i q_j}{r_{ij}}. \quad (1)$$

To describe the internal dynamics of the first hydration shell, a second potential called the IW1 is defined to deal with the interactions between the cation and the first-shell water molecules, $M^{m+}-(\text{H}_2\text{O})_1$ [19]. The following expression is used for IW1:

$$E_{\text{IW1}} = \frac{A_4^{\text{MO}_1}}{r_{\text{MO}_1}^4} + \frac{A_6^{\text{MO}_1}}{r_{\text{MO}_1}^6} + \frac{A_7^{\text{MO}_1}}{r_{\text{MO}_1}^7} + \frac{A_{12}^{\text{MO}_1}}{r_{\text{MO}_1}^{12}} + \sum_i^{\text{W}_1 \text{ sites}} \frac{q_{\text{M}} q_i}{r_{\text{Mi}}}. \quad (2)$$

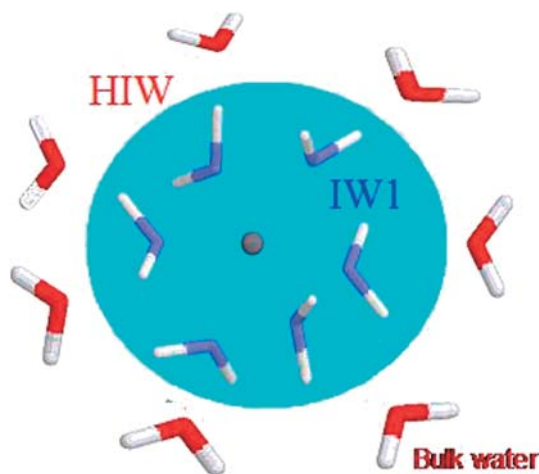


Fig. 1. Representation of the regions where the two ion-water interaction potentials are defined: ion-water of the first shell (IW1), and hydrated ion-water of the bulk (HIW)

The aqueous solution regions adopted as a result of the application of the hydrated ion model of an ionic solution are illustrated in Fig. 1. Two types of water molecules are defined. The first type of water molecules are those of the first hydration shell which are restricted to this region (in the course of the simulation), and interact with the bare cation through the IW1 potential, and with each other through a modified TIP4P potential where the charges and geometries are those derived from the quantum chemical computations of the hydrate. The second type of water molecules are those belonging to the bulk, which interact with the hydrated ion by means of the HIW potential, and with each other by means of the TIP4P water potential.

The degree of transferability of the interaction potentials among different hydrates was established previously by examining the cases of Al^{3+} , Mg^{2+} and Be^{2+} hydrates developed from the Cr^{3+} [18]. The same procedure was used here to obtain the HIW and IW1 potentials for Rh^{3+} . Further details about the methodology can be found elsewhere [16,17,18,19]. The following fitted parameters for rhodium interaction potentials were used:

$q_{\text{Rh}} = 2.1324$, $q_{\text{O}} = -1.0408$, $q_{\text{H}} = 0.5927$, $A_4^{\text{RhO}_1} = -30589$, $A_6^{\text{RhO}_1} = 244622.5$, $A_7^{\text{RhO}_1} = -287414.3$ and $A_{12}^{\text{RhO}_1} = 256799.961$. A_n coefficient values are given in $\text{kJ} \cdot \text{\AA}^n$ per mole and the q values are partial charges in fractions of e .

2.3 MD simulations

MD simulations were performed in the canonical ensemble (NVT) using periodic boundary conditions. Simulations were carried out at 298 K. A recently developed symplectic algorithm of the leapfrog type was applied to a system formed by rigid bodies described by the quaternion formalism. The integrator stability enabled us to use a timestep of 2 fs.

In all cases, the density was 0.997 g/cm^3 . Box side lengths, cutoff radii and total simulation times for production periods are detailed in Table 1. To test the behavior of the new terms included in the Ewald sum on the different types of properties, two simulations of $\text{Rh}^{3+}(\text{H}_2\text{O})_{500}$ were carried out: in the first one, a cutoff radius of 9 \AA and the 1-4-6-7-Ewald sum terms were applied; the second one used a cutoff radius of 12 \AA and only the 1-Ewald sum term. A simulation time of 1 ns was produced and the results of these two simulations were analyzed in detail, extracting trajectories and velocities of the molecules every 4 fs. For the rest of the systems, 250 ps of simulation time was produced. The r^{-n} terms which were included in the reciprocal space of the Ewald sum treatment are detailed in Table 1.

Long-range interactions were computed by the Ewald sum technique including the charged system term. Given the functional form of the intermolecular HIW and IW1 potentials (Eqs. 1, 2), a numerical improvement in estimating the total energy of the system can be achieved by extending the Ewald sum to the terms r^{-4} , r^{-6} and r^{-7} .

The mathematical details of the technique are described in an article by Williams [37]. In the real part, the energy terms are given by

$$V_{\text{real}} = \sum_n^\dagger \sum_{i=1}^N \sum_{j=i+1}^N \left\{ e^{-\alpha^2 |\mathbf{r}_{ij} + \mathbf{n}|^2} \left[A_4^{ij} \frac{1 + \alpha^2 |\mathbf{r}_{ij} + \mathbf{n}|^2}{|\mathbf{r}_{ij} + \mathbf{n}|^4} + A_6^{ij} \frac{1 + \alpha^2 |\mathbf{r}_{ij} + \mathbf{n}|^2 + \frac{\alpha^4}{2} |\mathbf{r}_{ij} + \mathbf{n}|^4}{|\mathbf{r}_{ij} + \mathbf{n}|^6} + A_7^{ij} \left(\frac{\alpha |\mathbf{r}_{ij} + \mathbf{n}|}{\sqrt{\pi}} \right) \times \left(\frac{2 + \frac{4}{3} \alpha^2 |\mathbf{r}_{ij} + \mathbf{n}|^2 + \frac{8}{15} \alpha^4 |\mathbf{r}_{ij} + \mathbf{n}|^4}{|\mathbf{r}_{ij} + \mathbf{n}|^7} \right) \right] + A_7^{ij} \frac{\text{erfc}(\alpha |\mathbf{r}_{ij} + \mathbf{n}|)}{|\mathbf{r}_{ij} + \mathbf{n}|^7} \right\} + A_{12}^{ij} \frac{1}{|\mathbf{r}_{ij}|^{12}}.$$

and

$$V_{\text{intra}} = - \sum_{m=1}^M \sum_{\kappa=1}^{N_m} \sum_{\lambda=\kappa+1}^{N_m} \left\{ \left(\frac{A_4^{\kappa\lambda}}{r_{\kappa\lambda}^4} + \frac{A_6^{\kappa\lambda}}{r_{\kappa\lambda}^6} + \frac{A_7^{\kappa\lambda}}{r_{\kappa\lambda}^7} \right) - e^{-\alpha^2 |\mathbf{r}_{\kappa\lambda}|^2} \left[A_4^{\kappa\lambda} \frac{1 + \alpha^2 |\mathbf{r}_{\kappa\lambda}|^2}{|\mathbf{r}_{\kappa\lambda}|^4} + A_6^{\kappa\lambda} \frac{1 + \alpha^2 |\mathbf{r}_{\kappa\lambda}|^2 + \frac{\alpha^4}{2} |\mathbf{r}_{\kappa\lambda}|^4}{|\mathbf{r}_{\kappa\lambda}|^6} + A_7^{\kappa\lambda} \left(\frac{\alpha |\mathbf{r}_{\kappa\lambda}|}{\sqrt{\pi}} \right) \times \left(\frac{2 + \frac{4}{3} \alpha^2 |\mathbf{r}_{\kappa\lambda}|^2 + \frac{8}{15} \alpha^4 |\mathbf{r}_{\kappa\lambda}|^4}{|\mathbf{r}_{\kappa\lambda}|^7} \right) \right] - A_7^{\kappa\lambda} \frac{\text{erfc}(\alpha |\mathbf{r}_{\kappa\lambda}|)}{|\mathbf{r}_{\kappa\lambda}|^7} \right\}.$$

In the reciprocal space, energy contributions are given by

$$V_{\text{recip}} = \frac{1}{V} \sum_{\mathbf{k} \neq 0} \left\{ \left[-\frac{\pi^2 \mathbf{k}}{2} \text{erfc} \left(\frac{\mathbf{k}}{2\alpha} \right) + \pi^3/2 \alpha e^{-\frac{\mathbf{k}^2}{4\alpha^2}} \right] \times \left[\sum_{i=1}^N A_4^{ii} + 2 \sum_{i=1}^N \sum_{j=i+1}^N A_4^{ij} \cos(\mathbf{k} \cdot \mathbf{r}_{ij}) \right] + \left[\frac{\pi^2}{24} \mathbf{k}^3 \text{erfc} \left(\frac{\mathbf{k}}{2\alpha} \right) + \frac{\pi^3/2}{6} \alpha e^{-\frac{\mathbf{k}^2}{4\alpha^2}} \left(\alpha^2 - \frac{\mathbf{k}^2}{2} \right) \right] \times \left[\sum_{i=1}^N A_6^{ii} + 2 \sum_{i=1}^N \sum_{j=i+1}^N A_6^{ij} \cos(\mathbf{k} \cdot \mathbf{r}_{ij}) \right] + \frac{\pi}{120} \left[(16\alpha^4 - 4\alpha^2 \mathbf{k}^2) e^{-\frac{\mathbf{k}^2}{4\alpha^2}} + \mathbf{k}^4 E_1 \left(\frac{\mathbf{k}^2}{4\alpha^2} \right) \right] \times \left[\sum_{i=1}^N A_7^{ii} + 2 \sum_{i=1}^N \sum_{j=i+1}^N A_7^{ij} \cos(\mathbf{k} \cdot \mathbf{r}_{ij}) \right] \right\}.$$

Correction terms to the energy due to the sheet and self-energy must be taken into account:

$$V_{\text{sheet}} = \frac{1}{V} \sum_{i=1}^N \sum_{j=1}^N \left[\pi^3/2 \left(\alpha A_4^{ij} + \frac{\alpha^3}{6} A_6^{ij} \right) + \frac{2}{15} \pi \alpha^4 A_7^{ij} \right],$$

$$V_{\text{self}} = - \left(\frac{\alpha^4}{4} \sum_{i=1}^N A_4^{ii} + \frac{\alpha^6}{12} \sum_{i=1}^N A_6^{ii} + \frac{8\alpha^7}{105\sqrt{\pi}} \sum_{i=1}^N A_7^{ii} \right).$$

In these formulae, erfc is the complementary error function, and is E_1 the exponential integral. The ‘‘dagged’’ summation indicates omission of site pairs i, j belonging to the same molecule if $\mathbf{n} = 0$. The rest of symbols have the following meaning: \mathbf{n} and \mathbf{k} are, respectively, the lattice and reciprocal lattice vector of a periodic array of MD cell images, k is the modulus of \mathbf{k} , i and j are absolute indices of interacting sites, m is the index of the molecules; κ and λ are indices of sites within a single molecule, N is the total number of sites, M is the total number of molecules, N_m is the number of sites on molecule m , A_n^{ij} is the coefficient of the r^{-n} potential term between sites i and j , \mathbf{r}_i is the Cartesian coordinate of site i , \mathbf{r}_{ij} is $\mathbf{r}_j - \mathbf{r}_i$, α , is the real versus the reciprocal space partition parameter, and V is the volume of the MD cell. Further details will be given in a forthcoming paper.

Table 1. Details of the simulations for the systems $[\text{Rh}(\text{H}_2\text{O})_6]^{3+} + (n-6) \text{H}_2\text{O}$

$n \text{ H}_2\text{O}$	$R_{\text{cutoff}}/\text{\AA}$	$L/\text{\AA}$	Inverse powers treated by Ewald	Simulation time/ps
50	5.9	11.865	1,4,6,7	250
100	7.3	14.688	1,4,6,7	250
200	9.0	18.338	1,4,6,7	250
500	9.0	24.749	1,4,6,7	1000
500	12.0	24.749	1	1000
1000	9.0	31.124	1,4,6,7	250
2500	12.0	42.194	1	250

MOLDY uses two sets of values of $\{\alpha, k_{\max}\}$: one for the Coulomb potential, and the other for other powers of r . The set of values chosen for r^{-n} ($n \neq 1$) was optimized for each box size according to standard criteria.

This new method opens the opportunity to decrease the cutoff radii of so-called short-ranged forces with minimal loss of accuracy. Simulations were performed using a developer version of the MD simulation code MOLDY [38] which is efficiently parallelized on a BEOWULF-type personal computer cluster.

3 Results and discussion

The potentials generated are tested in this section. The results derived from classical MD simulations which employed the new potentials are examined. From these results of the numerical simulations, the cation hydration is described.

3.1 Structural results

The radial distribution functions (RDF) of the Rh–O and Rh–H pairs obtained from the different simulations are shown in Fig. 2. Given that the simulations contain two types of water molecules (first-shell and bulk) the RDF plotted is the result of superimposing the corresponding two functions (Rh– X_I and Rh– X_{bulk}) for each pair (Rh–O and Rh–H). Given that these two functions describe the atomic distribution within two different regions (see Fig. 1), the final distribution obtained can be formally considered as the usual RDF.

The first Rh–O peak appears at the same distance for all simulations, 1.99 Å. It reflects a global small shortening of the mean value in solution with respect to the quantum mechanically optimized Rh–O distance in the hexahydrate. The latter is reproduced by a minimization

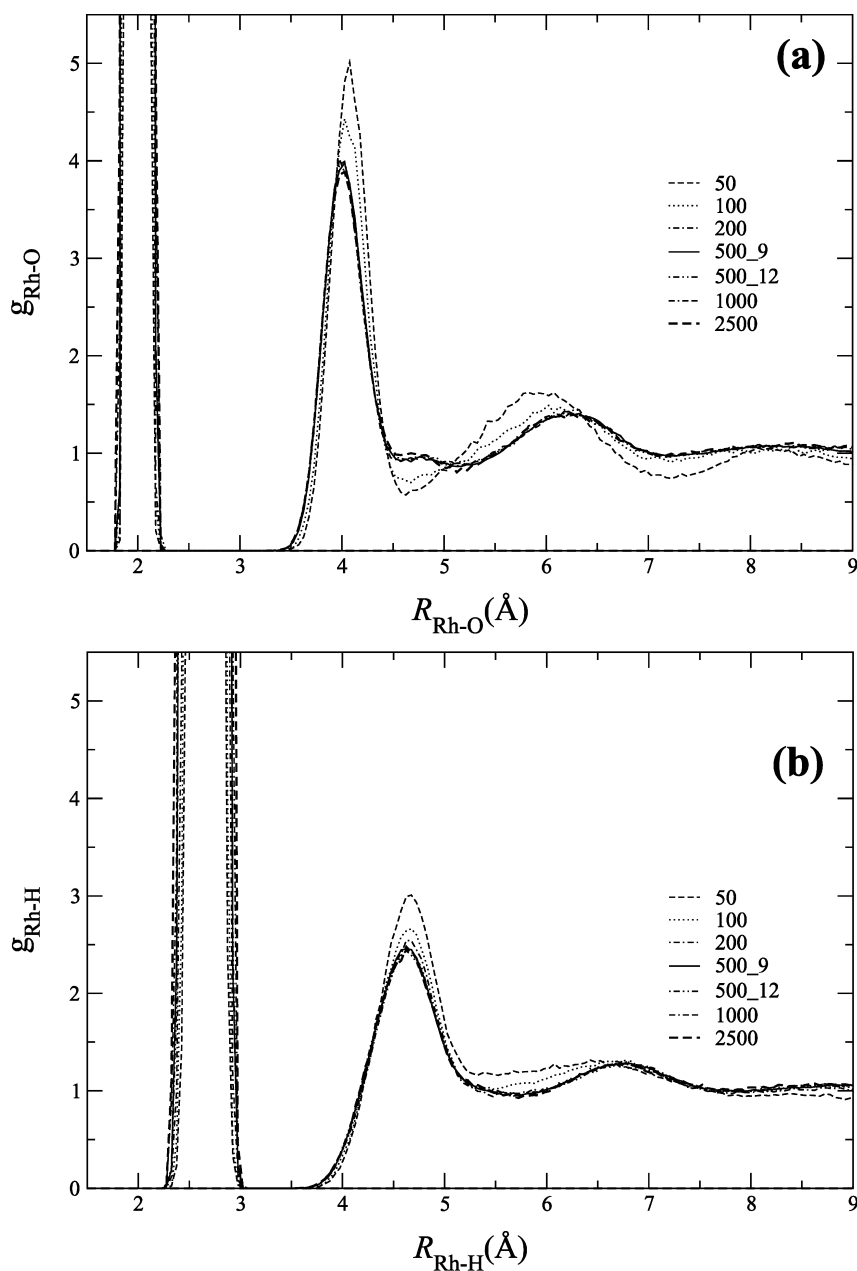


Fig. 2. Rh–O(a) and Rh–H(b) radial distribution functions obtained from simulations of the system $[\text{Rh}(\text{H}_2\text{O})_6]^{3+} + (n-6)(\text{H}_2\text{O})$, for $n = 50\text{--}2500$

of the hexahydrate using the potentials employed in the simulations. The observed shortening for the metal–oxygen distance has already been reported in previous works and points out the rather small effect of the condensed medium on this parameter [39]. This is the consequence of an almost complete cancellation of specific and bulk effects of the solvent on the hexahydrate geometry [40]. The Rh–O peak corresponding to the second hydration shell is centered at 4.02 Å and extends to a minimum placed at around 4.5 Å. The running integration number ascribes around 14 molecules to the second shell. The comparison of the second peak as a function of the system size shows a more defined second hydration shell when the number of water molecules is small (50/100). This is clearly visible from the height of the peak as well as from the minimum of the RDF in the region separating the second and third shells when going from 50/100 systems to the larger systems. This suggests that periodic boundary condition effects and long-range interaction treatment are not completely negligible for small boxes as they promote an enhancement of the water structure around the cation. For larger systems (200 water molecules or more) no difference in the RDF up to 9 Å is found. The different distributions observed for the small and big systems might be rationalized on the basis of the relative importance for the second hydration shell played by interactions with the hydrate and the bulk water. For the smallest system, bulk water is represented by only a few molecules (around 30), whereas in the case of the largest system this number increases up to around 2480. Nonetheless, periodic boundary condition effects could also contribute to the difference observed in the RDFs of the smaller systems. The structure-making character of this trivalent cation is illustrated by the presence of a well-defined and wider third peak centered around 6 Å.

Concerning the Rh–H RDFs, the peaks are wider than those corresponding to the Rh–O RDF even for the peak defining the first hydration shell. This fact is a consequence of the librational and rotational movements of water molecules which are affecting the hydrogen atoms more strongly than the oxygen ones. The well-defined second and third hydration shells are a consequence of the high degree of structure-making induced by the Rh^{3+} cation. The maxima are located at 2.67 and 4.63 Å. As already observed for Rh–O RDFs, the smaller systems (50/100) do not match the distribution of the rest of the systems, the convergence being achieved completely for systems with 500 or more water molecules and more.

Structural data available for Rh^{3+} aqueous solutions [22,41,42,43] agree quite well with those derived from our simulations. First-shell oxygen distances in the literature range from 2.02 to 2.04 Å. For the second shell the range covers 3.99–4.11 Å.

An additional structural analysis of the atomic distribution around the cation can be carried out by computing the spatial distribution functions of a given type of atom showing the 3D regions of higher probability [44]. This representation for the oxygen and hydrogen atoms of the first hydration shell as well as the oxygen atom belonging to the second hydration shell is

displayed in Fig. 3. Threshold values were set up to show surfaces including 50% of the total distribution. The study was done for the system with 500 water molecules and $R_{\text{cutoff}} = 9 \text{ \AA}$. These distributions clearly show the 3D local structure of the first and second hydration shells around the Rh^{3+} ion: first-shell oxygen atoms slightly fluctuate around their average position, whereas first-shell hydrogen atoms are more widespread than oxygen, due primarily to the rotation around the rhodium–oxygen axis. The small thickness of the white rings indicates that librations of water molecules have small amplitude. The second shell of oxygen atoms is represented by a quite homogeneous distribution in a much wider region. Both ringlike distributions reflect the well-defined hydrogen-bond network present in the first–second shell regions.

3.2 Energetic results

Size-dependency of the hydration energy was examined by studying Rh^{3+} in systems with different numbers of water molecules (from $n = 50$ to 2500). MD simulations within the canonical ensemble allow the estimation of the hydration energy of Rh^{3+} in water at 298K. In addition to simulations carried out for $\text{Rh}^{3+} + n\text{H}_2\text{O}$, a set of simulations of n TIP4P water molecules was performed under the same conditions. The definition of the HIW potential describes the average interaction energy of the $[\text{Rh}(\text{H}_2\text{O})_6]^{3+}$ cation with the bulk water, thus giving the main contribution to the hydration energy of the Rh^{3+} hexahydrate. The second intermolecular potential, IW1, gives the contribution to the hydration energy due to the interaction of the bare cation with the water molecules of the first shell. As far as this potential was fitted to the ab initio formation energy of this cluster, the addition of this second contribution to the total energy of the system enables the direct computation of the cation hydration energy

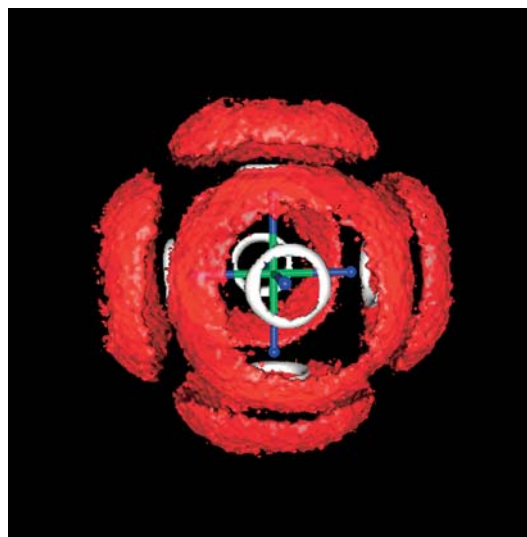


Fig. 3. Spatial distribution functions around Rh^{3+} for O_I (blue), H_I (white) and O_{II} (red)

once the water energy reference has been subtracted from the total energy of the corresponding simulation containing the cation. The computed energies with the associated standard deviations are summarized in Table 2. The experimentally estimated hydration enthalpy value for Rh^{3+} is -4521.4 kJ/mol [45,46]. Although, at first sight, an overestimation of 20% could be considered quite large, it is worth pointing out that first principles intermolecular potentials for highly charged cations are affected by extremely large many-body effects. As previously shown for the Cr^{3+} case, the inclusion of a polarizable water model improves to a great extent the hydration enthalpy estimation [47]. HIW and IW1 potentials provide a satisfactory way to deal with energy contributions present in the neighborhood of the metal ion, and the Rh^{3+} hydration energy estimation reinforces previous results obtained by the Monte Carlo method [16,47].

The hydration energies obtained for the different system sizes are quite similar, particularly considering the standard deviation associated with each value. This result proves the good energetic behavior of the Ewald sum treatment, which enables the use of systems as small as 50 or 100 water molecules to compute the hydration energy of a trivalent transition-metal cation. Several groups have already stressed this capability of the Ewald sum for monovalent and divalent ion cases [48,49]. Within the general agreement among the different systems studied, it is worth noting that a slight trend in ΔE with the increase of in the number of water molecules in the simulation box is observed. Further studies focusing on this point should clarify if the trend holds up when larger systems are simulated. Also, the origin of the good energy prediction for small systems (where periodic boundary conditions implicitly introduce some concentration effects) should be understood. In fact, it is striking that the RDFs seem to be more affected by the reduction of the box size than the hydration energy. Finally, the two simulations with 500 water molecules illustrate the statistically equivalent behavior of the total energy when coupling the cutoff radius to the inclusion of additional r^{-n} terms in the Ewald sum treatment. A quantification of this remark is the comparison of the long-range correction to the energy. The simulation using $R_{\text{cutoff}} = 9$ Å and 1-4-6-7-Ewald sum terms includes a correction of $+0.1$ kJ/mol, whereas in the other case, $R_{\text{cutoff}} = 12$ Å and 1-Ewald sum, the value is -465.0 kJ/mol.

Table 2. Hydration energy of the cation in the system $[\text{Rh}(\text{H}_2\text{O})_6]^{3+} + (n - 6) \text{H}_2\text{O}$ as a function of the number of water molecules n

$n \text{ H}_2\text{O}$	$\Delta E/(\text{kJ.mol})$
50	-5654 ± 86
100	-5667 ± 148
200	-5716 ± 196
500 ($R_{\text{cutoff}} = 9$ Å)	-5711 ± 328
500 ($R_{\text{cutoff}} = 12$ Å)	-5769 ± 317
1000	-5809 ± 428
2500	-5781 ± 562

3.3 Dynamical results

A set of dynamic quantities was computed for the simulation containing 500 water molecules and a cutoff radius of 9 Å. The structural results, previously discussed, converged for this system size. The analysis presented here pursues the dynamic characterization of the hydrated Rh^{3+} ion and its neighborhood. Some of the properties studied were also computed for the simulation having a 12-Å cutoff radius. The comparison between both sets of results extends the previous energetic and structural test to the case of dynamic properties between the simulation implementing the conventional Ewald treatment for the Coulombic term and that extending the methodology to the short-range r^{-4} , r^{-6} and r^{-7} contributions. The set of properties computed for the hydrated ion (metal ion and first shell water molecules) and the second hydration sphere water molecules is collected in Table 3. Unfortunately, the available experimental information characterizing the dynamics of Rh^{3+} aqueous solutions is scarce, so direct comparisons with our MD results are not possible for most of the properties studied. Nonetheless, comparisons with computed values of other inert hexahydrated trivalent metal ions point out the differential behavior for this metal ion.

3.3.1 Translational and librational motions

The mobility of the ion in terms of the self-diffusion coefficient D was estimated from the integration of the velocity autocorrelation function [6]. In both simulations, the hydrate shows the same mobility, $0.6 \times 10^{-5} \text{ cm}^2/\text{s}$, very similar to the observed ones for other hexacoordinated trivalent metal ions [18].

Power spectra of the ion and first-shell water molecules were obtained by means of the Fourier transform (FT) of the corresponding velocity autocorrelation function. The power spectra obtained are shown in Fig. 4. The spectral densities can be related with characteristic frequencies in the intermolecular region of the vibrational spectra [50,51]. Maxima located at 260 and 595 cm^{-1} are common for both the ion and water spectra. The unambiguous identification of these maxima with dynamic variables is not trivial. For that purpose, additional correlation functions connected with specific dynamic variables were analyzed by means of the corresponding FT. In particular, the evolution of metal ion–oxygen distances and oxygen–ion–oxygen angles was studied, among others. More details about this treatment can be found elsewhere [18]. On the basis of these studies, the previously mentioned peaks can be identified with a O–Rh–O bending mode (260 cm^{-1}) and with a characteristic Rh–O stretching frequency (595 cm^{-1}). For the other two main peaks observed in the $(\text{H}_2\text{O})_I$ spectrum, 380 and 515 cm^{-1} , only the maximum at lower frequency could be identified with an oxygen–oxygen stretching mode involving hexahydrate water molecules in trans positions. Experimentally, aqueous solutions containing Rh^{3+} have been studied by means of Raman spectroscopy [52]. A polarized band identified with the A_g symmetric stretching mode has

Table 3. Translational diffusion coefficients D (10^{-5} cm²/s), reorientational times, τ_l (ps) of order l ($l = 1, 2$) for the hydrate and the first-shell water molecules, and mean residence times, τ_{MRT} (ps), for water molecules in the second hydration shell for the simulation

Hydrate			(H ₂ O) _I			(H ₂ O) _{II}	
D_{ion}	τ_1	τ_2	$\tau_1^{\mu}/\tau_2^{\mu}$	$\tau_1^{\text{H-H}}/\tau_2^{\text{H-H}}$	$\tau_1^{\perp}/\tau_2^{\perp}$	$\tau_{\text{MRT}}^{t^*=0}$	$\tau_{\text{MRT}}^{t^*=2}$
0.6 ± 0.1 (0.6 ± 0.1)	69 ± 6	23 ± 4	$71 \pm 4/24 \pm 1$	$19 \pm 2/10 \pm 1$	$19 \pm 1/10 \pm 1$	9 (9)	18 (20)

been well characterized at 529 cm⁻¹. Although a normal mode analysis of the hexahydrate MD trajectory should be performed in order to identify the A_g mode frequency, the agreement between the experimental and theoretically estimated frequencies is fairly good. This fact and the close agreement also observed for other studied cases [19,18] where a similar strategy was applied reveals, in our opinion, a fine tuning of the balance of the HIW and IW1 forces.

3.3.2 Orientational dynamics

The well-defined behavior of the hydrate as a whole allows the study of its rotational behavior. A set of reorientational time correlation functions defined as

$$C_l^i(t) = \langle P_l(\vec{u}_i(0) \cdot \vec{u}_i(t)) \rangle$$

where P_l is the l th Legendre polynomial and \vec{u}_i is a unit vector that characterizes the orientation of the molecule, was computed. $C_l(t)$ values were obtained using a coordinate frame based on the molecule, and the reorientational times were obtained by fitting the long time decay of the function to a single exponential form. Functions with $l=1$ and $l=2$ may be related to spectroscopic measurements [6, 41, 53], such as IR and Raman line shapes (τ_1) and NMR relaxation times (τ_2). For the flexible hexahydrate, three Rh–O_{*l*} vectors, mutually perpendicular, were used. Because of the average symmetry of the complex, the three vectors are equivalent and, therefore, the values reported in Table 3 correspond to the averages of the three components. In the case of water molecules defining the first shell, a vector containing the dipole moment of the molecule, μ , the intramolecular hydrogen–hydrogen vector, H–H, and a third one perpendicular to the molecular plane, \perp , were used.

The rotational behaviour of the [Rh(H₂O)₆]³⁺ aqua-ion is similar to that found in other hexahydrates. τ_1 and τ_2 values are of the same order as ions like Cr³⁺ [19] or Al³⁺ [18], although slightly lower values are found for the rhodium case. Interestingly, the ratio $\tau_1/\tau_2 = 3$ is again found, confirming the adequacy of the Debye model [54] to describe the rotational dynamics of non-labile hydrated ions [17, 19].

The rotational motion of the first-shell solvent molecules reflects the strong influence of the metal cation. In particular, the reorientation of the water dipole moment vector is completely dominated by the reorientation of the hydrate itself. This fact should not be a surprise if one takes into account the strong ion–dipole orientation imposed by the metal ion. The other two components

containing 500 solvent molecules and a cutoff radius of 9 Å. Values in *parentheses* correspond to simulation with the same number of water molecules but with a 12Å cutoff radius

show smaller and virtually identical characteristic times. In all cases, the τ values obtained are much larger than the range of characteristic reorientational times of bulk water molecules [17] ($\tau_1 = 2.6$ – 3.7 ps, $\tau_2 = 1.6$ – 2.0 ps). The present analysis implies that the main water rotational motion contribution is around the dipole moment axis. The rotation of the dipole moment itself is effectively decoupled from the other two components and must be understood on the basis of the hydrate rotation.

3.3.3 Mean residence times

The last dynamic information retrieved from the simulation concerns the evaluation of the mean residence times of bulk water molecules in the second hydration shell. The mean residence time is based on the definition of a function, $n_{\text{ion}}(t)$, measuring the number of solvent molecules confined in a given region around the metal ion for a period of time t [55]. Excluding an initial period in which the function decays rapidly, $n_{\text{ion}}(t)$ follows an exponential form, $e^{-t/\tau}$, where τ represents a characteristic relaxation time of the persistence of the solvent molecules in the region considered. An additional parameter, t^* , defining the maximum transient period

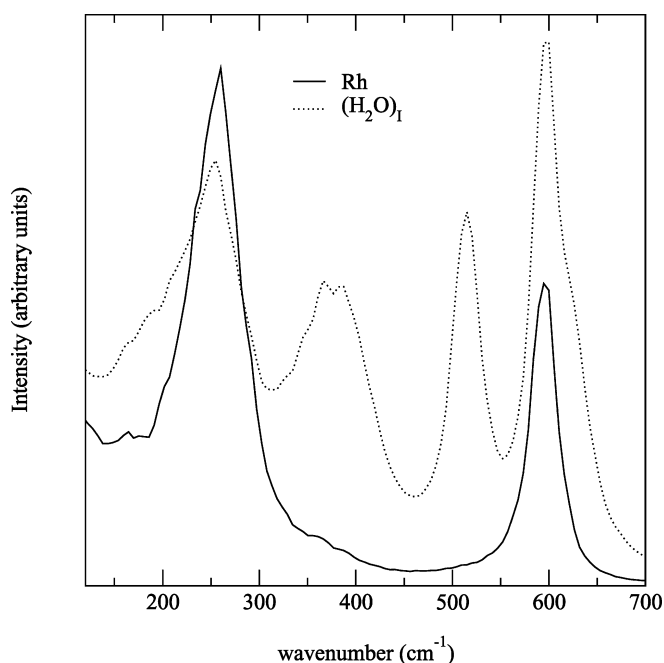


Fig. 4. Power spectra of [Rh(H₂O)₆]³⁺ corresponding to the simulation of the hydrate and 494 water molecules

that a molecule can leave the defined region without losing its ascription to it, must be taken into account when computing $n_{\text{ion}}(t)$. Values of 0 [56] and 2 ps [55] have previously been used in the literature to define a relevant range of mean residence times. It is interesting to note that both simulations analyzed yield the same range of values, 9–20 ps, showing again similar dynamic behavior of the particles for the two implementations already discussed. That mean residence time range is similar to the first-shell residence times of many monovalent and some divalent cations [15,41]. Again, for this property, no differential behavior is found for Rh^{3+} compared to Al^{3+} or Cr^{3+} . This fact reveals an important feature: the loss of specificity for the hydrated ion–bulk water interactions when dealing with long-lived hydrated ions of the same charge and coordination number. First-shell water molecules effectively buffer the ion–solvent interactions, bulk water molecules experiencing a very similar field regardless of the ion. At this point it is worth remembering that this result is obtained for ions in which the hydrate formation energies ($\Delta E = E_{[M(\text{H}_2\text{O})_6]^{3+}} - 6E_{\text{H}_2\text{O}} - E_{M^{3+}}$) can be as different as 400 kJ/mol and the ion–oxygen distance for the optimized hydrate structures differ by around 0.1 Å.

4 Concluding remarks

A set of potential parameters for the Rh^{3+} aquaion has been presented and tested by MD simulations. Good structural, energetic and dynamical behavior has been found, supporting the strategy followed.

The application of the Ewald sum strategy to the usually short-ranged terms (r^{-n} , $n = 4, 6, 7$) has shown that reduction of the cutoff radius is possible without altering dynamical, energetic and structural properties. This fact enables us to perform simulations with a number of water molecules as small as 50. The set of boxes probed shows that the structural properties (RDF) are more sensitive to the system size than the hydration energy, provided the extended Ewald treatment is used.

Acknowledgements. We are grateful to the Fundación Ramón Areces for financial support. ESM and KR thank the British Council and the Spanish MCYT for the Acción Integrada Hispano Británica (HB1999-0122). PJM acknowledges financial support from the Deutsche Forschungsgemeinschaft (Germany).

References

- Burgess J (1978) Metal ions in solution. Harwood, New York
- Conway BE (1981) Ionic hydration in chemistry and biophysics. Studies in physical and theoretical chemistry, Vol 12. Elsevier, Amsterdam
- Marcus Y (1986) Ion solvation. Wiley, Chichester
- Barthel JMG, Krienke H, Kunz W (1998) Physical chemistry of electrolyte solutions. Steinkopff, Darmstadt
- Clementi E (1990) Modern techniques in computational chemistry. Escom, Leiden, chap 1
- Allen MP, Tildesley DJ (1987) Computer simulation of liquids. Oxford University Press, Oxford
- Stone AJ (1996) The theory of intermolecular forces. Clarendon, Oxford
- Elrod NJ, Saykally RJ (1994) Chem Rev 94: 1975
- Curtiss LA, Halley JW, Hautman J, Rahman A (1987) J Chem Phys 86: 2319
- Frank HS, Evans MW (1945) J Chem Phys 13: 507
- Bockris JO, Reddy AKN (1998) Modern electrochemistry 1, 2nd edn. Plenum, New York
- Taube H (1954) J Phys Chem 58: 523
- Richens DT (1997) The chemistry of aqua ions. Wiley, Chichester
- Pappalardo RR, Sánchez Marcos E (1993) J Phys Chem 97: 4500
- Helm L, Merbach AE (1999) Coord Chem Rev 187: 151
- Pappalardo RR, Martínez JM, Sánchez Marcos E (1996) J Phys Chem 100: 11748
- Martínez JM, Pappalardo RR, Sánchez Marcos E, Refson K, Díaz-Moreno S, Muñoz-Páez A (1998) J Phys Chem B 102: 3272
- Martínez JM, Pappalardo RR, Sánchez Marcos E (1999) J Am Chem Soc 121: 3175
- Martínez JM, Pappalardo RR, Sánchez Marcos E (1998) J Chem Phys 109: 1445
- Merkling PJ, Muñoz-Páez A, Martínez JM, Pappalardo RR, Sánchez Marcos E (2001) Phys Rev B 64: 012201
- Merkling PJ, Muñoz-Páez A, Pappalardo RR, Sánchez Marcos E (2001) Phys Rev B 64: 092201
- Merkling PJ, Muñoz-Páez A, Sánchez Marcos E (2002) J Am Chem Soc 124: 10911
- Laurency G, Rapaport I, Zbinden D, Merbach AE (1991) Mag Res Chem 29: S45
- Plumb W, Harris GM (1964) Inorg Chem 3: 542
- Dolg M, Stoll H, Preuss H, Pitzer RM (1993) J Phys Chem 97: 5852, and modifications included at <http://www.emsl.pnl.gov:2080/forms/basisform.html>
- Kendall RA, Dunning TH Jr., Harrison RJ (1992) J Chem Phys 96: 6796
- Dunning TH Jr (1989) J Chem Phys 90: 1007
- Tomasi J, Persico M (1994) Chem Rev 94: 2027
- Miertus S, Scrocco E, Tomasi J (1981) Chem Phys 55: 117
- Cances E, Mennucci B, Tomasi J (1997) J Chem Phys 107: 3032
- Tomasi J, Mennucci B, Cances E (1999) J Mol Struct (THEOCHEM) 464: 211
- Frisch MJ, Trucks GW, Schlegel HB, Scuseria GE, Robb MA, Cheeseman JR, Zakrzewski VG, Montgomery JA Jr, Stratmann RE, Burant JC, Dapprich S, Millam JM, Daniels AD, Kudin KN, Strain MC, Farkas O, Tomasi J, Barone V, Cossi M, Cammi R, Mennucci B, Pomelli C, Adamo C, Clifford S, Ochterski J, Petersson GA, Ayala PY, Cui Q, Morokuma K, Malick DK, Rabuck AD, Raghavachari K, Foresman JB, Cioslowski J, Ortiz JV, Baboul AG, Stefanov BB, Liu G, Liashenko A, Piskorz P, Komaromi I, Gomperts R, Martin RL, Fox DJ, Keith T, AlLaham MA, Peng CY, Nanayakkara A, Challacombe M, Gill PMW, Johnson B, Chen W, Wong MW, Andres JL, Gonzalez C, Head-Gordon M, Replogle ES, Pople JA (1998) Gaussian, Pittsburgh, PA, Gaussian 98, revision A.9,
- Barone V, Cossi M (1998) J Phys Chem A 102: 1995
- Amovilli C, Mennucci B (1997) J Phys Chem B 101: 1051
- Sigfridsson E, Ryde U (1998) J Comput Chem 19: 377
- Besler BH, Merz KM, Kollman PA (1990) J Comput Chem 11: 431
- Williams DE (1993) In: Shmueli U (ed) International tables for crystallography, Kluwer, New York, vol. B
- Refson K (2000) Comput Phys Commun 126: 310
- Martínez JM, Pappalardo RR, Sánchez Marcos E (1997) J Phys Chem A 101: 4444
- Martínez JM, Pappalardo RR, Sánchez Marcos E, Mennucci B, Tomasi J (2002) J Phys Chem B 106: 1118
- Ohtaki H, Radnai T (1993) Chem Rev 93: 1157

42. Magini M, Licheri G, Paschina GG, Piccaluga G, Pinna G (1988) X-ray diffraction of ions in aqueous solutions: hydration and complex formation. CRC, Boca Raton, FL
43. Read MC, Sandström M (1992) *Acta Chem Scand* 46: 1177
44. Kusalik PG, Laaksonen A, Svishchev IM (1999) In: Balbuena PB, Seminario JM (eds) *Molecular dynamics. From classical to quantum methods*. Elsevier, Amsterdam, chap 3
45. Kurotaki K, Kawamura S (1993) *J Chem Soc Faraday Trans* 89: 3039
46. Marcus Y (1997) *Ion properties*. Dekker, New York
47. Martínez JM, Hernández-Cobos J, Saint-Martin H, Pappalardo RR, Ortega-Blake I, Sánchez Marcos E (2000) *J Chem Phys* 112: 2339
48. Hummer G, Pratt L, Garcia A (1996) *J Phys Chem* 100: 1206
49. Hummer G, Pratt L, Garcia A (1997) *J Chem Phys* 107: 9275
50. Irish DE, Brooker MH (1976) In: *Advances in infrared and Raman spectroscopies*, Vol 2, Heyden, London, chap 6
51. Lilley TH (1973) In: Franks F (ed) *Water—a Comprehensive treatise*, Vol 3. Plenum, New York, chap 6
52. Best SP, Beattie JK, Armstrong RS, Braitwaite GP (1989) *J Chem Soc Dalton Trans* 1771
53. Hertz HG (1973) In: Franks F (ed) *Water—a comprehensive treatise*, Vol 3 Plenum, New York, chap 7
54. Hansen JP, McDonald IR (1990) *Theory of simple liquids*, 2nd edn. Academic, London
55. Impey RW, Madden PA, McDonald IR (1983) *J Phys Chem* 87: 5071
56. Garcia AE, Stiller L (1993) *J Comput Chem* 14: 1396